Effect of Oscillatory Shear Deformation on Demixing Processes of Polymer Blends

Katsuo Matsuzaka,[†] Hiroshi Jinnai,[†] Tsuyoshi Koga,[†] and Takeji Hashimoto*[,†,‡]

Hashimoto Polymer Phasing Project, ERATO, JST, 15 Morimoto-cho, Shimogamo Sakyo-ku, Kyoto 606, Japan, and Department of Polymer Chemistry, Graduate School of Engineering, Kyoto University, Kyoto 606-01, Japan

Received August 12, 1996; Revised Manuscript Received November 20, 1996[⊗]

ABSTRACT: The influence of oscillatory shear deformation on spinodal decomposition (SD) processes in a blend of polybutadiene and polyisoprene has been investigated by *in-situ* observations of light scattering patterns. A large strain amplitude $\gamma_0 = 0.8$, with angular frequencies $\omega = 0.63$ and 6.3 rad/s, was imposed on the blend undergoing SD induced by a temperature jump from a homogeneous (or single phase) region to a thermodynamically unstable region. Comparing representative rates of the shear deformation (i.e., frequency ω and a maximum shear rate) with representative growth rates for SD (i.e., growth rate of concentration fluctuations in the early stage SD and that of domains in the later stage SD), the deformation used in the present study is expected to bring the system into a homogeneous state, based on an estimation in the simple shear flow case. In spite of this strong shearing criterion, SD still occurred at $\omega = 0.63$ rad/s: the phase-separated structure is affinely deformed in harmony with the shear strain phase and grows with time on a time scale longer than the cycle of the oscillatory deformation. In contrast, no remarkable sign of SD could be observed up to 80 min after the onset of SD under oscillatory shear deformation at $\omega = 6.3$ rad/s, although well-defined characteristic scattering of SD ("spinodal ring") can clearly be observed both in the absence and in the presence of the low-frequency shear ($\omega = 0.63$ rad/s) at the corresponding time scale.

I. Introduction

Phase transitions and critical phenomena of binary mixtures have been studied both theoretically and experimentally for many years. In recent years, much attention has been given to the influence of flow field, especially that of simple shear flow, on them.[1−29] Simple shear flow brings phase-separated simple liquid mixtures,[4−10] solutions of polymer blends (ternary mixtures of polymer A, polymer B, and solvent),[3,12−16] and polymer blends[17−25] into a single-phase state when the shear rate $\dot{\gamma}$ exceeds the growth rate of the concentration fluctuations.[4,13,16] On the contrary, shear flow can bring single-phase polymer solutions[1,26−29] and polymer blends[22,23] into phase separation when the elastic effect[30−32] plays an important role.

Suppose that a system composed of droplets of one fluid phase dispersed in another is subjected to simple shear flow. Large droplets burst due to the hydrodynamic forces exerted by the flow. However, small droplets collide and grow into larger droplets due to the thermodynamic forces of lowering the surface free energy. Thus the balance of these two effects determines the steady-state droplet size as a function of the shear rate $\dot{\gamma}$.[33−35] With increasing $\dot{\gamma}$, clusters of droplets align parallel to the flow, which results eventually in the percolated structure (the flow-induced cluster-to-percolation transition[35,36]). Recent experimental research revealed that a strong simple shear flow achieves a string-like phase-separated structure along the flow direction.[37]

The morphology of phase-separated structures under a flow field has also attracted considerable attention in recent years. Several studies[6,10,12,14,15,37,38] have been concerned with phase-separation processes via spinodal decomposition (SD) under simple shear flow, in which anisotropic SD was observed. This indicates that the phase-separated domains via SD were elongated along the flow direction. Simple shear flow also promoted collisions of domains along the flow direction, which consequently enhanced the domain coarsening.

A few articles examined the influence of both simple[39,40] and oscillatory shear flow[41−47] on a microphase-separated lamellar morphology of a diblock copolymer. They found that simple shear flow oriented the vectors normal to lamellar interfaces only parallel to the shear gradient direction[39,40] and that oscillatory shear flow, in contrast, induced two types of lamellar orientation, i.e., the normal vectors parallel to the shear gradient or to the vorticity direction (or the neutral direction), depending upon shearing frequency, amplitude of the shear strain, and quench depth from the order−disorder transition temperature of the system.[42−45] Besides the difference in the observed lamellar orientation between oscillatory and simple shear, it is worth noting that oscillatory shear yields much better lamellar orientation than simple shear.[39,40]

Thus, it is expected that shear may induce a morphological transition from the bicontinuous structure developed by SD in the absence of the flow field to a lamella-like structure. Especially oscillatory shear may induce better orientation of the phase-separating lamella-like structure of a binary mixture than simple shear. Little attention, however, has been given so far to the influence of oscillatory shear on the structures of binary mixtures. In the present study, we focus on the influence of oscillatory shear on the phase separation process of polybutadiene (PB) and polyisoprene (PI) blends.

II. Experimental Methods

A binary mixture of polybutadiene (PB) and polyisoprene (PI) with a near-critical composition (50 wt %/50 wt %) was chosen. Molecular characteristics of PB and PI used in the

* To whom correspondence should be addressed.
[†] Hashimoto Polymer Phasing Project, ERATO, JST.
[‡] Kyoto University.
[⊗] Abstract published in *Advance ACS Abstracts,* January 15, 1997.

S0024-9297(96)01212-0 CCC: $14.00

Table 1. Molecular Characteristics of Polybutadiene (PB) and Polyisoprene (PI) Used for This Study

sample code	$M_w \times 10^{-4}$ [a]	M_w/M_n [a]	microstructure[b]			
			cis-1,4	*trans*-1,4	1,2	3,4
PB	5.8	1.2	28	56	16	
PI	10.1	1.3	70.4	22.1		7.5

[a] Measured using size exclusion chromatography. [b] Measured by IR spectroscopy.

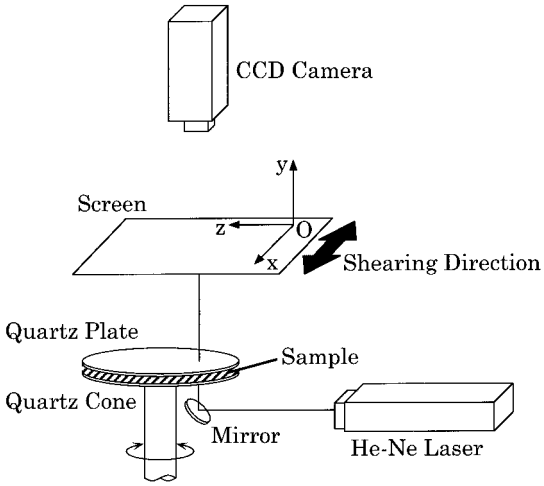

Figure 1. Flow-SALS optical system with the Cartesian coordinate used in the present work. The O*x* axis is parallel to the shearing direction, the O*y* axis to the shear gradient direction, and the O*z* axis to the vorticity direction. The propagation of the incident beam is along the O*y* axis, and the two-dimensional light scattering pattern is detected on a screen parallel to the O*xz* plane.

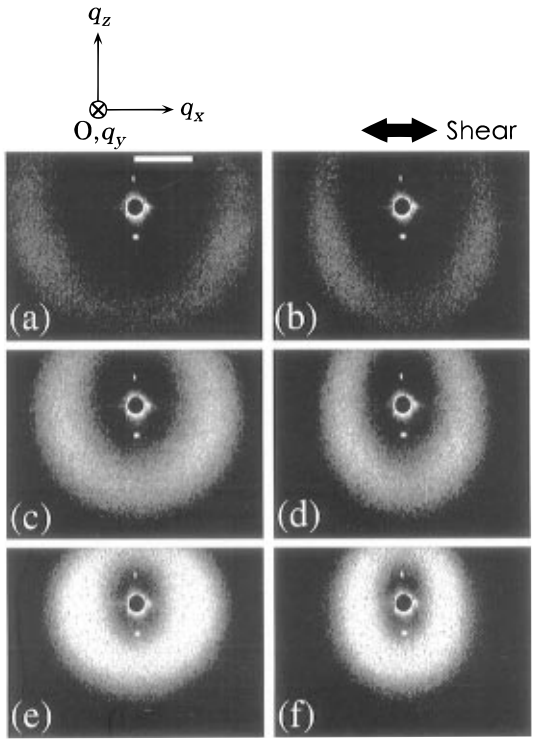

Figure 2. Time evolution of light scattering patterns obtained *in situ* by the CCD camera in the SD process of the PB/PI mixture under the oscillatory shearing of $\omega = 0.63$ rad/s at 50 °C: 50 min (a, b), 70 min (c, d), 100 min (e, f); (left column: a, c, and e) at a strain phase $\phi = 0$, (right column: b, d, and f) at $\phi = \pi/2$. The white bar shown in (a) corresponds to $q = 5.0 \times 10^{-4}$ nm^{-1}.

present study are summarized in Table 1. The mixtures were dissolved in toluene to prepare homogeneous solutions containing 10 wt % polymer. The solutions were first filtered through a Millipore film having an average pore size of 0.45 μm and then cast into thin films by slowly evaporating the solvent for 5 days at about 20 °C. Films thus obtained were further dried in a vacuum oven for 1 day. The PB/PI blend has a lower critical solution temperature (LCST) type phase diagram with a critical temperature T_s of 25.5 °C in the absence of shear.[48] The SD processes of the blend in the absence of external fields have already been reported elsewhere.[48,49]

Time-resolved light scattering measurements were performed with a flow small-angle light scattering (flow-SALS) apparatus. The apparatus used in the present study has been described elsewhere in detail.[50] It consists of a cone and plate with radii of 40 mm and a cone angle of 1.0°, which was placed in a temperature-controlled (±0.3 °C) enclosure. A He−Ne laser with a wavelength of 632.8 nm was used as an incident beam source. The incident beam propagates along the velocity gradient. Scattering was imaged on a screen placed normal to the incident beam, as shown in Figure 1, whose intensity distribution was taken with a two-dimensional charge coupled device (CCD) camera.

We applied oscillatory shear deformation to the blend, sandwiched between the cone and plate, undergoing SD induced by a temperature jump (T-jump) from $T = 21$ °C (a single-phase region) to 50 °C (a spinodal region). We chose a strain amplitude, γ_0, of 0.8, and frequencies, ω, of 0.63 and 6.3 rad/s. The frequencies used in our experiments at $T = 50$ °C are in the terminal region in the viscoelastic spectrum for both components of the blend. The SD processes with the oscillatory shearing were followed *in situ* and *at real time* by time-resolved light scattering.

III. Results

A. Low-Frequency Behavior: Time Evolution of Scattering Pattern at $\omega = 0.63$ rad/s. The time evolution of the scattering pattern was taken after the onset of SD at $T = 50$ °C with the oscillatory shear deformation at $\omega = 0.63$ rad/s, which is referred to as low-frequency behavior hereafter. The scattering at a given strain phase ϕ, which is defined by $\phi \equiv \sin^{-1}(\gamma/\gamma_0)$, was almost identical with that at the same ϕ after one period of the shearing cycle ($2\pi/\omega = 10$ s), although the scattering oscillated with ϕ and evolved with time t. That is to say, the time evolution of the scattering caused by the domain growth via SD is much slower than one period of the shearing cycle. Thus, we can ignore the change in the scattering caused by the domain growth via SD within one shearing cycle. In the present paper, we consider t and ϕ as independent variables for simplicity, though ϕ depends on t in a strict sense.

Figure 2 shows the time evolution of the scattering $I(\mathbf{q},t;\phi)$ taken at representative strain phases: $\phi = 0$ (left column) and $\phi = \pi/2$ (right column). Here, $\mathbf{q}$ denotes a scattering wave vector whose magnitude is defined by $q \equiv (4\pi/\lambda)\sin(\theta/2)$, where θ and λ are the scattering angle and the wavelength of radiation in the medium, respectively. Parts a and b of Figure 2 show the scattering obtained at $t = 50$ min after the quench (reduced time $\tau = 68.1$). Here τ is defined by

$$\tau \equiv t/t_c \tag{1}$$

where $t_c = 44.0$ s is a characteristic time of the mixture at 50 °C in the absence of shear evoluted from the phase separation kinetics in the early stage SD.[49] Figure 2a shows that the scattering intensity distribution $I(\mathbf{q},t;0)$ had approximately circular symmetry with respect to the incident beam axis (directionally independent in our q plane). This is often called the "spinodal ring", which

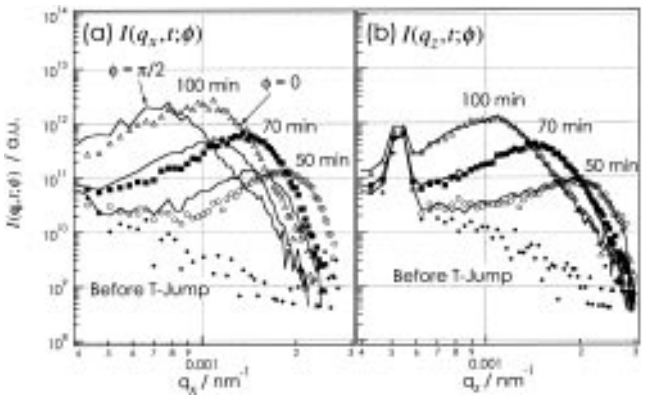

Figure 3. Time evolution of scattering intensity $I(\mathbf{q},t;\phi)$ as a function of the magnitude q of $\mathbf{q}$ at $\omega = 0.63$ rad/s: (a) $I(q_x,t;\phi=0)$ and $I(q_x,t;\phi=\pi/2)$ (along the q_x direction, i.e., parallel to the shear direction); (b) $I(q_z,t;\phi=0)$ and $I(q_z,t;\phi=\pi/2)$ (along the q_z direction, i.e., perpendicular to the shearing direction). Dots represent the scattering in the single-phase state before the T-jump. Symbols and solid lines show scattering at the strain phase $\phi = 0$ and at $\phi = \pi/2$, respectively. Excess scattering at $q_z = 5.3 \times 10^{-4}$ nm^{-1} in (b) is an artificial scattering due to the multiple reflection of the incident beam from the cone-and-plate cell.

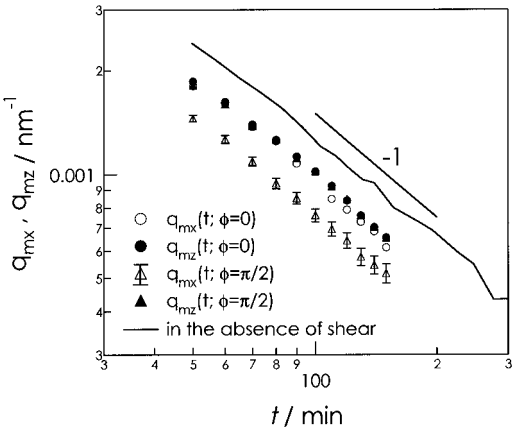

Figure 4. Time dependence of q_m's at $\omega = 0.63$ rad/s, including that in the absence of shear for comparison: $q_{mx}(t;0)$ (○); $q_{mz}(t;0)$ (●); $q_{mx}(t;\pi/2)$ (△); $q_{mz}(t;\pi/2)$ (▲). It should be noted that the data ○, ●, and ▲ almost completely coincide.

is characteristic of SD in the absence of applied fields. The wave number q_m, at which maximum intensity (i.e., the spinodal ring) is detected, is related to a characteristic wavelength Λ of a periodic structure through $\Lambda \equiv 2\pi/q_m$. Since Λ grows with t, q_m moves to smaller q in an intermediate and a late stage SD. The circular spinodal ring in Figure 2a means that the phase-separated structure is isotropic.

In Figure 2b, on the other hand, the spinodal ring became an ellipse whose short axis was parallel to the shear direction, indicating that the spinodally decomposed domains were elongated along the shear direction at the maximum shear strain of $\phi = \pi/2$. The peak position of the pattern in the direction parallel to the shear direction oscillated with ϕ, while that perpendicular to the shear was almost stationary, i.e., independent of ϕ. Thus the shear deformation oscillatorily elongated the phase-separated structure along the shear direction. The same trend was observed at other t as shown in Figure 2.

From the left column in Figure 2, we note that the width of the spinodal ring along the shear direction at $\phi = 0$ is broader than that in the direction perpendicular to the shear direction, although the peak position q_m is independent of the direction. Hence, the size distribution of the domain depends on the direction; i.e., the phase-separated structure got disturbed especially along the shearing direction, while the characteristic domain size was independent of the direction.

Figure 3 shows the time evolution of the scattering intensity distribution $I(\mathbf{q},t;\phi)$ as a function of $\mathbf{q}_{\|} = (q_x,0,0)$ (part a: along the shearing direction) and $\mathbf{q}_{\perp} = (0,0,q_z)$ (part b: along the neutral direction) at $\phi = 0$ (data shown by symbols) and at $\phi = \pi/2$ (data shown by solid lines), each of which was obtained by averaging the scattered intensity around the respective sectors (azimuthal angle of ±5°) centered around the Ox or Oz axis. For simplicity, we denote $I(\mathbf{q}_{\|},t;\phi)$ and $I(\mathbf{q}_{\perp},t;\phi)$ as $I(q_x,t;\phi)$ and $I(q_z,t;\phi)$, respectively. The peak position moves to smaller q and the peak intensity increases with t in both the q_x and q_z directions, which is characteristic of SD. At a given t, $I(q_x,t;\phi)$ oscillated with ϕ, whereas $I(q_z,t;\phi)$ was independent of ϕ, which indicates that the shear deforms the phase-separated structure along the shear direction but does not in the direction perpendicular to the shear direction.

Figure 4 shows the time dependence of $q_{mx}(t;0)$, $q_{mx}(t;\pi/2)$, $q_{mz}t;0)$, and $q_{mz}(t;\pi/2)$. Here the subscript m in front of the coordinate in q denotes the wave number q at which the maximum intensity was observed. It is clear, as we have seen qualitatively earlier, that the wave number $q_{mz}(t;\phi)$ was independent of ϕ, while $q_{mx}(t;\phi)$ depended on ϕ at a given t. All quantities were found to decrease with a slope of −1, indicating that the hydrodynamic effect on the domain growth is significant.[51,52] This demonstrates that the coarsening mechanism at $\omega = 0.63$ rad/s is the same as that in the absence of shear except for the fact that the oscillatory deformation accelerates the SD process. The time dependences of $q_{mx}(t;0)$ and $q_{mz}(t;0)$ are almost identical, which again shows that the phase-separated structure is nearly isotropic at $\phi = 0$. However, $q_{mx}(t;\pi/2)$ got smaller than $q_{mz}(t;\pi/2)$, meaning that at $\phi = \pi/2$ the domain size in the shear direction was larger than that in the direction perpendicular to the shear direction.

B. High-Frequency Behavior: Time Evolution of Scattering Pattern at $\omega = 6.3$ rad/s. We applied the oscillatory shear deformation at $\omega = 6.3$ rad/s, which is referred to as high-frequency behavior hereafter, with the strain amplitude $\gamma_0 = 0.8$ just after the onset of SD at 50 °C. We note that we were not able to detect any scattering implying an occurrence of SD for 80 min after the T-jump (Figure 5a), although a well-defined spinodal ring can be already observed at 80 min both in the absence of shear and in the low-frequency case. We stopped applying the oscillatory shear deformation at $\phi = 0$ and at 80 min ($\equiv t_0$) after the T-jump. After cessation of shear, the scattering was taken. Figure 5 shows the time evolution of the light scattering patterns. Only Figure 5a shows the scattering pattern under the oscillatory shear, while the others show those after cessation of shear in which circular spinodal ring can be observed.

The time dependence of q_m after cessation of shear is plotted in Figure 6, where the time change in q_m in the absence of shear is also included for comparison (the solid line). Curves a, b, and c are the same q_m data obtained after the cessation of shear at $\omega = 6.3$ rad/s except for the definition of time. We defined the time of the T-jump as $t = 0$ in curve a and the time at cessation of shear as t' ($\equiv t - t_0$) = 0 in curve b. We will discuss curve c later.

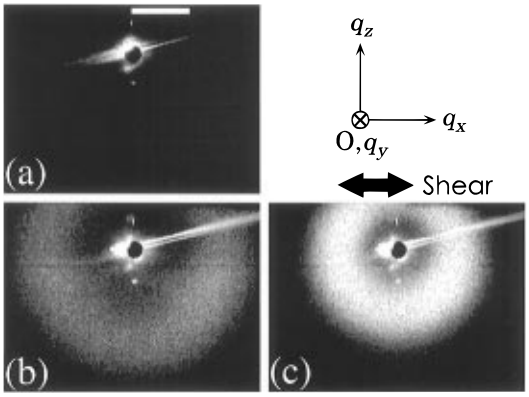

Figure 5. Time evolution of light scattering patterns obtained *in situ* by the CCD camera for the SD process of the PB/PI mixture at $\omega = 6.3$ rad/s: (a) 80 min (0 min) just before the cessation of shearing, (b) 120 min (40 min), and (c) 160 min (80 min) after the *T*-jump (and after the cessation of the shear in parentheses). The white bar shown in (a) corresponds to $q = 5.0 \times 10^{-4}$ nm^{-1}.

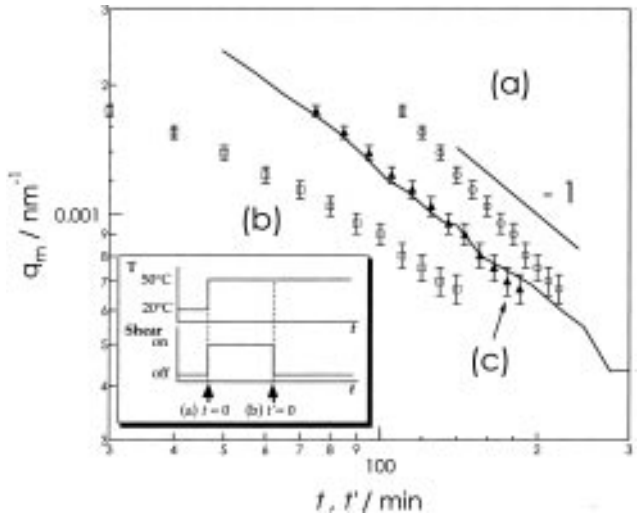

Figure 6. Time dependence of q_m after cessation of oscillatory shear of $\omega = 6.3$ rad/s in comparison with that in the absence of the shear (solid line). Circles (a), squares (b), and triangles (c) are the same experimental data after the cessation of oscillatory shear except for the definition of time t. Time at the *T*-jump is defined as $t = 0$ for curve a, and time at the cessation of shear as t' ($\equiv t - t_0$) = 0 for curve b, where t_0 (=80 min) denotes the duration of the shearing. We define the time as $t'' \equiv t' + t_0'$ in curve c, where $t_0' = 45$ min. The inset is a schematic illustration showing the definition of t.

In both cases, the power law dependence of q_m on t was not -1, which is contrary to what was found for the SD processes both in the absence of shear and in the low-frequency case. Comparing the time dependence of q_m in the absence of shear, curve a indicates that the dynamical evolution of the domain was slowed down by applying the high-frequency oscillatory shear deformation for 80 min. Curve b implies that the state just after cessation of shear was different from that before the *T*-jump in the absence of shear, i.e., a thermodynamically single-phase state. It is plausible that the mixture after shearing for 80 min had a certain phase-separated structure.

IV. Discussion

A. Comparison of Rate of Shear Deformation and Growth Rate. It is useful to estimate the rate of the shear deformation and the growth rate of the concentration fluctuations; if the former exceeds the latter, the system would be brought into a homogeneous (or single phase) state. This is true for simple shear and has already been reported by Beysens et al.[7,8] and Hashimoto et al.[12,13,16]

There are two kinds of characteristic rate to be considered: the frequency ω of the oscillation and the shear rate $\dot{\gamma}(\phi)$ oscillates with ϕ. We use the maximum shear rate $\dot{\gamma}_{max} = \gamma_0\omega$ as a characteristic shear rate. Thus we obtian $\dot{\gamma}_{max} = 0.50$ and 5.0 rad/s for $\omega = 0.63$ and 6.3 rad s^{-1}, respectively.

There are also two kinds of the growth rate of the concentration fluctuations. The first one is $1/t_c$, where t_c is a characteristic time of the early stage SD. The characteristic time t_c is given by

$$t_c = [D_{app} q_m^2(0)]^{-1} \tag{2}$$

where D_{app} is the collective diffusivity and $q_m(0)$ is the wave number of the dominant mode of the concentration fluctuations in the early stage of SD. The second growth rate to be considered is a growth rate of the Fourier component of the phase-separated structure with wave number q, $\Gamma(q)$, which is given by (see Appendix A)

$$\Gamma(q) \equiv C\frac{\sigma}{\eta}q \tag{3}$$

where η is the shear viscosity of the system, σ is the interfacial tension, and C is a constant.[52,53] The light scattering experiments in the late stage SD of the PB/PI mixture showed that

$$q_m(t)^{-1} = C\frac{\sigma}{\eta}t \tag{4}$$

with the value of $C(\sigma/\eta) \cong 1.2 \times 10^{-2}$ nm/s.[49] The fastest growth rate Γ_{max} of the phase-separated structure is the growth rate of the smallest domain. For simplicity, we assume that the smallest domain size is $2\pi/q_m(0)$ and then we obtain

$$\Gamma_{max} = C\frac{\sigma}{\eta}q_m(0) \tag{5}$$

Based on eqs 2 and 5, we obtain $1/t_c = 0.023$ s^{-1} and $\Gamma_{max} = 2.1 \times 10^{-6}$ s^{-1}, respectively. Here we use parameters characterizing the early stage of SD at $T = 50$ °C from ref 49: $D_{app} = 75.8$ nm^2/s and $q_m(0) = 1.73 \times 10^{-4}$ nm^{-1}.

Let us first compare the rate of the shear deformation with the growth rate of the concentration fluctuations in the case of low frequency. Both the frequency $\omega = 0.63$ rad/s and the maximum shear rate $\dot{\gamma}_{max} = 0.5$ s^{-1} are much larger than both the growth rate of the concentration fluctuations $1/t_c = 0.023$ s^{-1} and the fastest domain growth rate $\Gamma_{max} = 2.1 \times 10^{-6}$ s^{-1}. Therefore, if the simple shear flow of $\dot{\gamma} = 0.5$ s^{-1} were applied to the system, it would be large enough to wipe out the concentration fluctuations. It is worthwhile to point out that the phase separation occurred under the oscillatory shear deformation with such a large shear rate, as shown in Figure 2. This indicates that the estimation of the critical shear rate in the simple shear case cannot be applicable to the oscillatory shear case because the magnitude of the strain is finite in the oscillatory shear case while it steadily increases for simple shear. Further investigation on the origin of SD under the oscillatory shear deformation will be left for future work.

B. Change in Scattering Profiles with Strain Phase at Low Frequency ($\omega = 0.63$ rad/s). As the

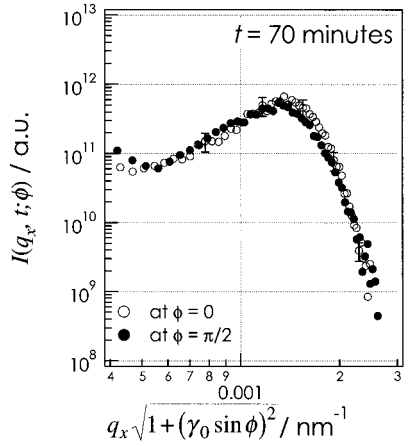

Figure 7. Plot of $I(q_x,t;\phi)$ against $q_x[1 + (\gamma_0 \sin \phi)^2]^{1/2}$. Open and filled circles show $I(q_x,t;\phi)$ at $\phi = 0$ and at $\phi = \pi/2$, respectively.

shearing cycle is much shorter than the characteristic time scale of the domain growth, the domain is expected to be deformed affinely in a time scale of shearing cycles (~10 s). Assuming that we can ignore the change in scattering caused by the domain growth in a shearing cycle, scattering intensity $I(q_x,t;\phi)$ and $I(q_z,t;\phi)$ can be written by (see Appendix B)

$$I(q_x,t;\phi) = I(q_x[1 + (\gamma_0 \sin \phi)^2]^{1/2},t;\phi=0) \quad (6)$$

$$I(q_z,t;\phi) = I(q_z,t;\phi=0) \quad (7)$$

Therefore a plot of the scattering intensity along q_x at a given ϕ, $I(q_x,t;\phi)$, against $q_x[1 + (\gamma_0 \sin \phi)^2]^{1/2}$ and $I(q_z,t;\phi)$ at a given ϕ against q_z should be independent of ϕ. Figure 7, obtained from the data shown in Figure 3a, shows the plot of $I(q_x,t;\phi)$ against $q_x[1 + (\gamma_0 \sin \phi)^2]^{1/2}$ at $t = 70$ min after the onset of shear and SD. $I(q_x,t;\pi/2)$ plotted in this way falls onto $I(q_x,t;0)$, the scattered intensity profile at $\gamma = 0$. The same results were obtained at other t. Thus we conclude that the domain was affinely deformed within one period of shearing, $2\pi/\omega$.

C. Functional Form of the Scattering Function at Low Frequency ($\omega = 0.63$ rad/s). Here we shall concentrate on the functional form of the scattering function in the late stage SD. It is well-known that the dynamical scaling hypothesis holds in the late stage SD in the absence of shear, which indicates that the domain growth is dynamically self-similar. In many experiments, this property has been investigated by using the scaled structure factor (i.e., scaled scattered intensity vs scaled scattering vector). It has already been observed that the dynamical scaling hypothesis holds for our system in the absence of shear in the same time range as that in the present study.[49]

Although we also want to study the scaling property under oscillatory shear deformation, it is difficult to obtain the invariant of $I(\mathbf{q},t;\phi)$ which is needed in the normalization of $I(\mathbf{q},t;\phi)$, because the scattering intensity depends on the direction of the wave vector. Therefore, for the sake of simplicity, we use the following normalized scattering intensity: $\tilde{I}(\tilde{\mathbf{q}},t;\phi) \equiv I(\mathbf{q},t;\phi)/I(\mathbf{q}_m,t;\phi)$, where $\tilde{\mathbf{q}} \equiv \mathbf{q}/|\mathbf{q}_m(t)|$ and $\mathbf{q}_m$ is the wave vector along $\mathbf{q}$ at which maximum intensity is detected. Figure 8 shows the time dependence of the normalized scattering intensity $\tilde{I}(\tilde{q}_x,t;\phi) \equiv \tilde{I}(\tilde{\mathbf{q}}=(\tilde{q}_x,0,0),t;\phi)$ and $\tilde{I}(\tilde{q}_z,t;\phi) \equiv \tilde{I}(\tilde{\mathbf{q}}=(0,0,\tilde{q}_z),t;\phi)$ as a function of the normalized scattering vector $\tilde{\mathbf{q}}$ along the q_x and q_z axes. According

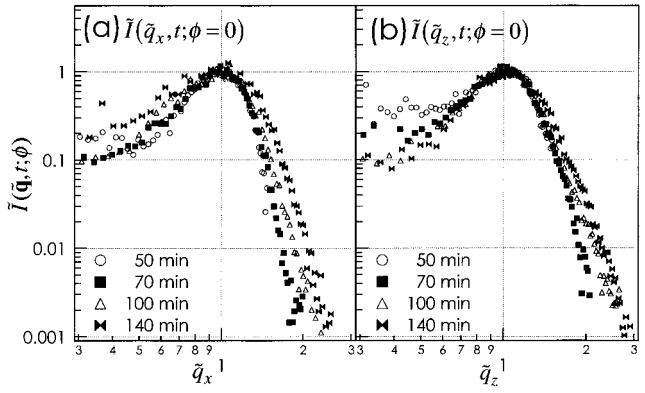

Figure 8. Time evolution of the normalized scattering intensity $\tilde{I}(\tilde{\mathbf{q}},t;\phi)$ as a function of normalized scattering vector $\tilde{\mathbf{q}}$ at $\omega = 0.63$ rad/s: (a) $\tilde{I}(\tilde{q}_x,t;0)$ vs $\tilde{q}_x \equiv q_x/q_{mx}$; (b) $\tilde{I}(\tilde{q}_z,t;0)$ vs $\tilde{q}_z \equiv q_z/q_{mz}$.

to our definition, $\tilde{q}_x \equiv q_x/q_{mx}$ and $\tilde{q}_z \equiv q_z/q_{mz}$, where q_{mx} and q_{mz} are, respectively, q_x and q_z at which $I(q_x,t;\phi)$ and $I(q_z,t;\phi)$ became maximum. It is obvious that both $\tilde{I}(\tilde{q}_x,t;\phi=0)$ and $\tilde{I}(\tilde{q}_z,t;\phi=0)$ were not invariant with t, but rather became broader with t, indicating that the oscillatory shear deformation made the size distribution of the domain broader. This tendency is more remarkable in the direction parallel to the shear direction than that perpendicular to the shear direction regardless of ϕ, i.e., $\phi = 0$ or $\pi/2$.

D. Possible Scenario for Structure at High Frequency ($\omega = 6.3$ rad/s). In the case of the high-frequency oscillatory shear, no distinct sign of the scattering was observed as shown in section IIIB. As Onuki et al. and Beysens et al. pointed out, simple shear flow would increase the single-phase region of the phase diagram.[4,7] If the system was brought into the homogeneous state by the shear flow, the growth of the domain after cessation of shear should be similar to that in the absence of shear if we use $t' \equiv t - t_0$ instead of t (curve B in Figure 6). However, our experimental results showed that the growth observed in the time scale of t' after cessation of shear was faster than that in the absence of shear (see Figure 6). This implies that the system was not in the same single-phase state as that in the absence of shear. Hence a certain structure should have already existed under oscillatory shear.

Let us assume that the structure at the cessation of shear, i.e., at $t = 80$ min, had the same structure as that at a certain time t_0' in the absence of shear. If this is the case, the time dependence of q_m for the PB/PI blend at $\omega = 6.3$ rad/s should be the same as that for the mixture in the absence of shear after an adequate time shift. This was tried and shown as curve c in Figure 6, in which q_m was plotted against $t'' \equiv t' + t_0'$. Here $t_0' = 45$ min. Curve c nicely fell onto q_m for the mixture in the absence of shear (i.e., the solid line), which may explain that the structure at $t = 80$ min at $\omega = 6.3$ rad/s corresponds to that at 45 min in the absence of shear. We note here, however, that there may be other effects of shear on the structure, i.e., shift of the phase diagram that leads to the change of the fluctuation amplitude and the orientation of domains. Those will be described in the following paragraphs.

There may be possible explanations for the experimental results presented above. First, shear shifted the phase diagram so that the quench depth $\Delta T \sim |T_s - T|$ at $\omega = 6.3$ rad/s became smaller than that at $\omega = 0.63$ rad/s, which made the SD process for the high frequency slower than that for the low frequency. If this is the

case, the spinodal ring would eventually be seen at times later than 80 min. This should be confirmed in future work.

Secondly, a nearly stationary two-phase state was achieved due to the dynamical balance between the two mechanisms: the thermodynamical force tends to promote the domain growth while the shear deformation tends to burst these domains and restrict their size. The stationary two-phase domains were small so that the scattering from them appeared in the q range outside our experimental one. Such a phenomenon has been reported for a polymer blend solution under simple shear flow.[13,16,35]

Thirdly, the planar orientation of domains might be achieved with their interfaces normal to the direction of shear gradient. In this case, the system scatters little light on our q plane. As for block copolymer systems, it has already been observed that oscillatory shear leads to orientation of lamella with their interfaces normal to the shear gradient.[39,40,42−45,47]

Finally, we point out the possibility that homogenization and phase separation alternately occurred depending on the magnitude of the shear rate. In contrast to the simple shear case, in oscillatory shear, the shear rate depends on the strain phase: $\dot{\gamma} = \gamma_0\omega \cos(\phi)$. Therefore, homogenization occurs when the magnitude of the shear rate $|\dot{\gamma}|$ exceeds the critical shear rate $\dot{\gamma}_c$, while phase separation takes place when $|\dot{\gamma}| < \dot{\gamma}_c$. In other words, the system experiences homogenization and phase separation in a cycle. The structure at 80 min may be formed under the competition of these two opposite effects.

V. Conclusion

We have performed *in-situ* light scattering experiments on spinodal decomposition (SD) processes of a binary mixture of polybutadiene and polyisoprene under oscillatory shear deformation, with frequencies ω of 0.63 and 6.3 rad/s and with the large strain amplitude, γ_0, of 0.8. The characteristic shear rates (i.e., the shearing frequency and the maximum shear rate) for both frequencies are much larger than the growth rate of the concentration fluctuations.

In spite of this estimation, the spinodal ring appeared at $\omega = 0.63$ rad/s, implying that SD took place under such oscillatory shear deformation. The scattering pattern oscillates with applied shear strain within one period of shearing cycle, which is found to be explained by the affine deformation of the domain by the shearing. For a longer time scale compared to the period of the oscillatory shear, the growth law of domains is the same as that in the absence of shear, while the dynamical scaling law for the scattering intensity did not hold under the oscillatory shear deformation at $\omega = 0.63$ rad/s: the scaled structure factor becomes broad with time.

In contrast, at $\omega = 6.3$ rad/s, we were not able to detect any scattering implying an occurrence of SD for 80 min after the T-jump in the q range covered in our experiments, although a well-defined spinodal ring was observed in this time scale after the onset of SD both in the absence of shear and at $\omega = 0.63$ rad/s. After cessation of shear, we observed an appearance and a shrinking of a circular spinodal ring, indicating an occurrence of SD. However, the time dependence of the characteristic wave number is different from that in the absence of shear, indicating that there is a certain unidentified structure at 80 min which differs from structures in the single-phase region.

Acknowledgment. The authors thank Dr. H. Watanabe for helpful discussions.

Appendix A

We define the growth rate Γ of the domains with characteristic length $l(t)$ as

$$\Gamma \equiv \frac{1}{l}\frac{\mathrm{d}l}{\mathrm{d}t} \tag{A1}$$

In the late stage SD in binary fluids with the full hydrodynamic interaction effect, l is given by

$$l = 2\pi C\frac{\sigma}{\eta}t \tag{A2}$$

where η is the shear viscosity of the system, σ is the interfacial tension, and C is a constant.[51−53] Using $q = 2\pi/l$, the growth rate $\Gamma(q)$ for the q Fourier mode is given by

$$\Gamma(q) = C\frac{\sigma}{\eta}q \tag{A3}$$

Appendix B

Here, we consider how the scattering function changes when each point $\mathbf{r}$ is transformed to $\mathbf{r}'$, according to

$$\mathbf{r}' = \mathbf{E}\cdot\mathbf{r} \tag{B1}$$

where $\mathbf{E}$ is a deformation gradient tensor.

Let us consider the initial state of the polymer blend A/B by the local concentration of component A, $\varphi(\mathbf{r})$. The initial scattering function $I_0(\mathbf{q})$ from the system before deformation is given by the Fourier transformation of a pair correlation function $g(\mathbf{r}) = \langle\delta\varphi(\mathbf{r}+\mathbf{r}_0)\delta\varphi(\mathbf{r}_0)\rangle$,

$$I_0(\mathbf{q}) = \int g(\mathbf{r}) \exp(-\mathrm{i}\mathbf{q}\cdot\mathbf{r})\, \mathrm{d}\mathbf{r} \tag{B2}$$

where $\mathbf{q}$ is a wave vector, $\langle\#\rangle$ denotes a spatial average of quantity # under constant $\mathbf{r}$, and $\delta\varphi(\mathbf{r}) = \varphi(\mathbf{r}) - \langle\varphi\rangle$. When affine deformation $\mathbf{E}$ is applied to the system, the local concentration $\varphi(\mathbf{r}')$ is given by

$$\varphi(\mathbf{r}') = \varphi(\mathbf{r}) \tag{B3}$$

Hence, the scattering function $I(\mathbf{q})$ from the system is given by

$$\begin{aligned} I(\mathbf{q}) &= \int g(\mathbf{r}') \exp(-\mathrm{i}\mathbf{q}\cdot\mathbf{r}')\, \mathrm{d}\mathbf{r}' \\ &= \int g(\mathbf{r}) \exp(-\mathrm{i}\mathbf{q}\cdot\mathbf{E}\cdot\mathbf{r})|\mathbf{E}|\, \mathrm{d}\mathbf{r} \\ &= |\mathbf{E}| I_0(\mathbf{q}\cdot\mathbf{E}) \end{aligned} \tag{B4}$$

where $|\mathbf{E}|$ is the determinant of $\mathbf{E}$.

Consider the case in which affine deformation with the shear strain γ is applied to the system. The deformation gradient tensor $\mathbf{E}$ is

$$\mathbf{E} = \begin{pmatrix} 1 & \gamma & 0 \\ 0 & 1 & 0 \\ 0 & 0 & 1 \end{pmatrix} \tag{B5}$$

and

$$\mathbf{q}\cdot\mathbf{E} = (q_x, \gamma q_x + q_y, q_z) \tag{B6}$$

When the system has an isotropic structure before shearing, the scattering function $I_0(\mathbf{q})$ can be written

as a function of the magnitude of the scattering vector

$$q = (q_x^2 + q_y^2 + q_z^2)^{1/2} \quad \text{(B7)}$$

therefore, $I_0(\mathbf{q}\cdot\mathbf{E})$ is represented by $I_0([q_x^2 + (\gamma q_x + q_y)^2 + q_z^2]^{1/2})$. Since we observed the scattering pattern in the xz plane, $q_y = 0$. In this case

$$I(\mathbf{q}) \equiv I(q_x,0,q_z) = I_0([(1+\gamma^2)q_x^2+q_z^2]^{1/2}) \quad \text{(B8)}$$

which leads to

$$I(q_x) \equiv I(q_x,0,0) = I_0(q_x[1 + \gamma^2]^{1/2}) \quad \text{along the } q_x \text{ axis} \quad \text{(B9)}$$

$$I(q_z) \equiv I(0,0,q_z) = I_0(q_z) \quad \text{along the } q_z \text{ axis} \quad \text{(B10)}$$

The scattering functions $I_0(\mathbf{q})$ and $I(\mathbf{q})$ correspond to $I(\mathbf{q},t;\phi=0)$ and $I(\mathbf{q},t;\phi)$ for our experiment, respectively, with $\gamma = \gamma_0 \sin \phi$. Thus we obtain eqs 6 and 7 in the text.

References and Notes

(1) Larson, R. G. *Rheol. Acta* **1992**, *31*, 497.
(2) *Flow-Induced Structure in Polymers*; Nakatani, A. I., Dadmun, M. D., Eds.; ACS Symposium Series 597; American Chemical Society: Washington, DC, 1995.
(3) Silberberg, A.; Kuhn, W. *J. Polym. Sci.* **1954**, *13*, 21.
(4) Onuki, A.; Kawasaki, K. *Ann. Phys. (N.Y.)* **1979**, *121*, 456.
(5) Onuki, A.; Yamazaki, K.; Kawasaki, K. *Ann. Phys. (N.Y.)* **1981**, *131*, 217.
(6) Onuki, A. *Phys. Rev. A* **1986**, *34*, 3528.
(7) Beysens, D.; Gbadamassi, M.; Boyer, L. *Phys. Rev. Lett.* **1979**, *43*, 1253.
(8) Beysens, D.; Gbadamassi, M. *J. Phys. Lett.* **1979**, *40*, L565.
(9) Beysens, D.; Gbadamassi, M.; Moncef-Bouanz, B. *Phys. Rev. A* **1983**, *28*, 2491.
(10) Beysens, D.; Perrot, F. *J. Phys. Lett.* **1984**, *45*, L31.
(11) Hamano, K.; Yamashita, S.; Sengers, J. V. *Phys. Rev. Lett.* **1992**, *68*, 3579.
(12) Takebe, T.; Hashimoto, T. *Polym. Commun.* **1988**, *29*, 261.
(13) Takebe, T.; Sawaoka, R.; Hashimoto, T. *J. Chem. Phys.* **1989**, *91*, 4369.
(14) Waldow, D. A.; Nakatani, A. I.; Han, C. C. *Polymer* **1992**, *33*, 4635.
(15) Nakatani, A. I.; Ban, Y.-B.; Han, C. C. *Polym. Mater. Sci. Eng.* **1992**, *67*, 327.
(16) Hashimoto, T.; Takebe, T.; Asakawa, K. *Physica A* **1993**, *194*, 338.
(17) Mazich, K. A.; Carr, S. H. *J. Appl. Phys.* **1983**, *54*, 5511.
(18) Katsaros, J. D.; Malone, M. F.; Winter, H. H. *Polym. Bull.* **1986**, *16*, 83.
(19) Kornfield, J. A.; Fuller, G. G.; Pearson, D. S. *Macromolecules* **1989**, *22*, 1334.
(20) Zawada, J. A.; Ylitalo, C. M.; Fuller, G. G.; Ralph, H. C.; Long, T. E. *Macromolecules* **1992**, *25*, 2894.
(21) Hindawi, I.; Higgins, J. S.; Galambos, A. F.; Weiss, R. A. *Macromolecules* **1990**, *23*, 670.
(22) Hindawi, I.; Higgins, J. S.; Weiss, R. A. *Polymer* **1992**, *33*, 2522.
(23) Mani, S.; Malone, M. F.; Winter, H. H.; Halary, J. L.; Monnerie, L. *Macromolecules* **1991**, *24*, 5451.
(24) Horst, R.; Wolf, B. A. *Macromolecules* **1992**, *25*, 5291.
(25) Horst, R.; Wolf, B. A. *Macromolecules* **1993**, *26*, 5676.
(26) Ver Strate, G.; Philippoff, W. *J. Polym. Sci., Polym. Lett. Ed.* **1974**, *12*, 267.
(27) Wolf, B. A. *Makromol. Chem.* **1980**, *1*, 231.
(28) Rangel-Nafaile, C.; Metzner, A. B.; Wissbrun, K. F. *Macromolecules* **1984**, *17*, 1187.
(29) Hashimoto, T.; Fujioka, K. *J. Phys. Soc. Jpn.* **1991**, *60*, 356.
(30) Helfand, E.; Fredrickson, G. H. *Phys. Rev. Lett.* **1989**, *62*, 2648.
(31) Onuki, A. *Phys. Rev. Lett.* **1989**, *62*, 2427.
(32) Doi, M.; Onuki, A. *J. Phys. II (Fr.)* **1992**, *2*, 1631.
(33) Taylor, G. I. *Proc. R. Soc. London* **1932**, *A138*, 41.
(34) Taylor, G. I. *Proc. R. Soc. London* **1934**, *A146*, 501.
(35) Hashimoto, T.; Takebe, T.; Fujioka, K. In *4th Nishinomiya−Yukawa Symposium on Theoretical Physics*; *Dynamics and Patterns in Complex Fluids*; Onuki, A., Kawasaki, K., Eds.; Springer: Heidelberg, 1990; pp 86−99.
(36) Hashimoto, T.; Matsuzaka, K.; Fujioka, K., in preparation.
(37) Hashimoto, T.; Matsuzaka, K.; Moses, E.; Onuki, A. *Phys. Rev. Lett.* **1995**, *74*, 126.
(38) Imaeda, T.; Onuki, A.; Kawasaki, K. *Prog. Theor. Phys.* **1984**, *71*, 16.
(39) Balsara, N. P.; Hammouda, B.; Kesani, P. K.; Jonnalagadda, S. V.; Straty, G. C. *Macromolecules* **1994**, *27*, 2566.
(40) Balsara, N. P.; Hammouda, B. *Phys. Rev. Lett.* **1994**, *72*, 360.
(41) Hadziioannou, G.; Mathis, A.; Skoulios, A. *Colloid Polym. Sci.* **1979**, *257*, 136.
(42) Koppi, K. A.; Tirrell, M.; Bates, F. S.; Almdal, K.; Colby, R. H. *J. Phys. II (Fr.)* **1992**, *2*, 1941.
(43) Koppi, K.; Tirrell, M.; Bates, F. S. *Phys. Rev. Lett.* **1993**, *70*, 1449.
(44) Gupta, V. K.; Krishnamoorti, R.; Kornfield, J. A.; Smith, S. D. *Macromolecules* **1995**, *28*, 4464.
(45) Gupta, V. K.; Krishnamoorti, R.; Chen, Z.-R.; Kornfield, J. A.; Smith, S. D. Satkowski, M. M.; Grothaus, J. T. *Macromolecules* **1996**, *29*, 875.
(46) Winter, H. H.; Scott, D. B.; Gronski, W.; Okamoto, S.; Hashimoto, T. *Macromolecules* **1993**, *26*, 7236.
(47) Okamoto, S.; Saijo, K.; Hashimoto, T. *Macromolecules* **1994**, *27*, 5547.
(48) Hashimoto, T.; Takenaka, M.; Jinnai, H. *J. Appl. Crystallogr.* **1991**, *24*, 457.
(49) Takenaka, M.; Hashimoto, T. *J. Chem. Phys.* **1992**, *96*, 6177.
(50) Kume, T.; Asakawa, K.; Moses, E.; Matsuzaka, K.; Hashimoto, T. *Acta Polym.* **1995**, *46*, 79.
(51) Siggia, E. D. *Phys. Rev. A* **1979**, *20*, 595.
(52) Koga, T.; Kawasaki, K. *Physica A* **1993**, *196*, 389.
(53) Kawasaki, K.; Ohta, T. *Physica A* **1983**, *118*, 175.

MA961212C